Pim J. de Vink[1#], Auke A. Koops[1#], Giulia D'Arrigo[1,2#], Gabriele Cruciani[3], Francesca Spyrakis[2*], Luc Brunsveld[1*]

1.Laboratory of Chemical Biology, Department of Biomedical Engineering and Institute for Complex Molecular Systems, Eindhoven University of Technology, P.O. Box 513, 5600MB Eindhoven, The Netherlands.
2. Department of Drug Science and Technology, University of Turin, via Giuria 9, 10125 Turin, Italy.
3. Department of Chemistry, Biology and Biotechnology, University of Perugia, Via Elce di Sotto 8, 06123, Perugia, Italy.
#Authors contributed equally

*Correspondence: francesca.spyrakis@unito.it; l.brunsveld@tue.nl

Content

Materials and Methods

Commercial origin of ligands and coregulators

The FAM-MED1 labeled coregulator peptide (FAM-NTKNHPMLMNLLKDNPAQD-*CONH$_2$*)) was bought from Invitrogen, (Thermofisher scientific, lot nr.: 2159072C). The Ac-MED1 coregulator peptide (*Ac*-NTKNHPMLMNLLKDNPAQD-*CONH$_2$*) was bought from Gen-script.
Rosiglitazone and Tesaglitazar were bought from Sigma-Aldrich**;** Troglitazone, Pioglitazone, Pemafibrate and Glabridin from MedChemExpress; Ciglitazone and Bezafibrate from Abcam; MRL24 from Focus Biomolecules; Telmisartan from TOCRIS.

Protein expression and purification

E.coli BL21 DE3 with PPARγ-LBD with N-terminal His-tag on a pET15b vector were incubated (37 ^{0} C) overnight in 3x30mL autoclaved LB medium (10 g/L peptone, 5 g/L yeast extract, 10 g/L NaCl and 30 µg/ml ampiciline, MiliQ). Next day the small cultures were transferred to separate 2 L LB medium and incubated at 37 ^{0}C until OD_{600} reached 0.6. Expression was induced using 0.1 mM IPTG for 18h at 18 ^{0}C. Cells were harvested by centrifuge for 10 mins at 15.000x g. Pellet was resuspended in 10 ml/mg lysis buffer (50 mM Tris, 300 mM NaCl, 35 mM imidazole, 5 mM $MgCl_2$, pH 8.0 and 1 μL/10 mL benzoase) and lysed twice in a homogenizer at a minimum pressure of 15.000 psi. The lysate was centrifuged again, 30 min at 40.000x g. A prepacked Ni-NTA column was equilibrated with 2 CV (10 mL) of lysis buffer. The supernatant was loaded and washed again with 2 CV of lysis buffer. Protein was eluted using 100 mM imidazole in 50 mM Tris, 300 mM NaCl and 2 mM BME. The fractions were combined and dialyzed in 4 L 25 mM HEPES, 100 mM NaCl, 2 mM $MgCl_2$, 4 mM BME and 10 % w/v glycerol for 2 hours, after which dialysis fluid was refreshed and left for another 2h. Finally, the protein was dialyzed against 2 L 25 mM HEPES, 100 mM NaCl, 2 mM $MgCl_2$,1 mM TCEP and 10 % w/v glycerol. Protein was concentrated using an Amicon ultra 15 (10-kDa cut-off) spin filter to a final concentration of 5.09 mg/ml and stored at -80 ^{0}C. Purity and mass were confirmed by using a High Resolution LC-MS system consisting of a Waters ACQUITY UPLC I-Class system coupled to a Xevo G2 Quadrupole Time of Flight (Q-ToF). The system was comprised of a Binary Solvent Manager and a Sample Manager with Fixed-Loop (SM-FL). The protein was separated (0.3 mL/min) by the column (Polaris C18A reverse phase column 2.0 x 100 mm, Agilent) using a 15% to 75% acetonitrile gradient in water supplemented with 0.1% v/v formic acid before analysis in positive mode in the mass spectrometer. Deconvolution of the m/z spectra was done using the MaxENT I algorithm in the Masslynx v4.1 (SCN862) software

2D Fluorescence anisotropy assays

All Fluorescence anisotropy assays were performed using a filter-based microplate reader (Tecan Infinite F500) using a filterset (λex:485 nm/20 nm, λem:535 nm/25 nm).
Plates were prepared via two subsequent serial dilutions, as previously been described[12]. In summary, for protein titration, first the ligands were serially diluted in dimethyl sulfoxide (DMSO) from a 10 mM stock, after which each concentration was transferred to a separate Eppendorf tube containing FA buffer (10 mM HEPES, 150 mM NaCl, 0.01% TWEEN-20 and 0.1% w/v bovine serum albumin, pH 7.4) and FAM-labeled coregulator peptide (MED1: FAM-NTKNHPMLMNLLKDNPAQD-*CONH$_2$*) for a concentration series of 400 μM till 0.097 μM ligand, 20 nM coregulator and 4% DMSO.

First column of each row of a low-volume 384-well black plate (Corning, #25916024) was filled with 10 μl of this mix, where the bottom three served as DMSO control. The rest of the Eppendorf mix was diluted 2x with FA buffer for a final concentration series of 200 μM till 0.046 μM ligand, 10 nM coregulator and 2% DMSO and 10 μl were added to each well of the appropriate row. 10 μl of 145 μM PPARγ-LBD was added to the first column of each row and subsequently mixed and diluted over the plate. For ligand titrations, a solution of protein and coregulator as diluted first, followed by a titration with the ligand keeping all concentration equal.

Binary coregulator affinity (K_D^I) and EC_{50}s were determined using Origin software. Cooperativity analysis was performed as previously described[1] (see supporting information detailed derivation).

Isothermal titration calorimetry

The final dialysis fluid from protein expression was frozen as 2 mL aliquots to serve as ITC buffer. Protein and ligand were diluted in this buffer to reported concentration and DMSO was added to match the DMSO concentration in cell and syringe. Samples were degassed for 10 min prior to measurement at 450 mmHg. The reference cell was filled with 300 µl degassed MilliQ water and sample cell with 300 μl of protein mixture. Syringe is loaded with at least 200 ul ligand sample. Measurements were performed on an Affinity ITC LV (TA instruments), with injection size set to 4 μl, stirring speed of 125 rpm and temperature at 25 ^{0}C. The initial data was processed and analyzed in NanoAnalyze v3.11. The baseline was corrected, after which a blank constant model was fitted to correct for the heat of injection. Subsequently an independent model was fitted, which the software uses to report the thermodynamic binding properties. For the analysis of the triplicate experiments with tesaglitazar, rosiglitazone and MED1 a different set-up was used. The raw data was loaded into NanoAnalyze and converted to a xml file. Subsequently this data was loaded in NITPIC v2.0.0a. Baseline determination and isotherm reconstruction via SVD was performed fully automated by NITPIC.[3] Reconstructed isotherm was saved as .xp file and loaded in SEDPHAT v15.2b. Supplemental experimental parameters were added in the file and the appropriate model was selected (Hetero-Association or triple complex). After an initial estimate of parameters, the model was fitted through the date points fitted alternating the Simplex and Levenberg-Marquardt algorithm to solve for the non-linear least squares until converged. Reported confidence intervals were obtained by generating a one-dimensional error surface projection based on F-statistics. All reported intervals are 95% confidence intervals. For visualization of the data, graphs were created in GUSSI.[4]

MD simulations

The crystal structure of rosiglitazone and SRC1 in complex with PPARγ (PDB code: 5YCP[5]) was used to build the ligand-bound and the apo states through the removal of the coregulator and of both the coregulator and the ligand, respectively. The Prime module[6,7] within the Schrodinger suite was used to fill in the missing part of the protein corresponding to the Ω loop (residues 262-272). The coregulator-bound state and the ternary complex with MED1 were built by merging the co-activator coordinates, retrieved from the PDB 6ONJ[8], respectively with the apo and the ligand-bound states, previously prepared. Molecular Dynamics simulations were performed using GROMACS version 4.6.1.[9] Systems were solvated in an octahedron box using TIP3P[10] water models and the standard AMBER ff14sb force field[11] was used to assign all protein parameters. Partial charges were assigned to the ligand using the restrained electrostatic surface potential (RESP) approach,[12] as implemented in the BiKi Life Science software suite[13] (http://www.bikitech.com). Subsequently, the four systems were first submitted to 5000 steps of energy minimization with the steepest descent algorithm and the coregulator-bound complexes were further minimized with the conjugate gradient algorithm for 10000 steps. To reach the temperature and pressure equilibrium conditions, seven equilibration steps were performed: 15 ps under the NVT ensemble at 50K, 100K, 150K, 200K, 250K and 300K and 5 ps under the NPT ensemble (time step: 2 fs). Finally, the four systems were simulated under the NVT ensemble for 1 μs.

Derivation of mathematical model and numerical solution

Supporting Figure S12 depicts the scheme of equilibria involved in protein-protein interaction stabilization via sequential addition of coregulatory (C, blue) and ligand (L, in orange) to a receptor (R, in gray protein via pathway A or pathway B, ligand and peptide respectively. The peptide-ligand binds to a receptor with K_D^{I}, in the presence of a stabilizer this affinity is altered to K_D^{III}. Similarly, the stabilizer binds with an intrinsic affinity K_D^{II}, and an enhanced affinity K_D^{IV} when the peptide is already bound.

To establish the model, let us define the following quantities:

R_{tot} : total concentration of PPARγ receptor in mol·L^{-1}
C_{tot}: total concentration of labeled coregulator in mol·L^{-1}
L_{tot}: total concentration of ligand in mol·L^{-1}
K_D^{I}: dissociation equilibrium constant for the binding of the coregulator to PPARγ monomer in mol·L^{-1}
K_D^{II}: dissociation equilibrium constant for the binding of the ligand to PPARγ in mol·L^{-1}
K_D^{III}: dissociation equilibrium constant for the binding of the coregulator to PPARγ in complex with ligand in mol·L^{-1}
K_D^{IV}: dissociation equilibrium constant for the binding of the ligand to PPARγ in complex with the coregulator in mol·L^{-1}
α: dimensionless cooperativity factor
[R]: free concentration PPARγ mol·L^{-1}
[C]: free concentration labeled partner in mol·L^{-1}
[L]: free concentration coregulator ligand in mol·L^{-1}
[RC]: concentration PPARγ•coregulator complex in mol·L^{-1}
[RL]: concentration PPARγ•ligand complex in mol·L^{-1}
[RLC]: concentration PPARγ•ligand•coregulator complex in mol·L^{-1}

We also constructed three mass-balance equations, describing the total receptor, ligand and coregulator concentrations (Eq. 1–3).

$$R_{tot} = [R] + [RL] + [RC] + [RLC] \quad (1)$$

$$L_{tot} = [L] + [RL] + [RLC] \quad (2)$$

$$C_{tot} = [C] + [RC] + [RLC] \quad (3)$$

Now, we write down the equilibrium equations of the dissociation constant K_Ds, and its related species. (Eq. 4–7).

$$K_D^{I} = \frac{[R] * [C]}{[RC]} \quad (4)$$

$$K_D^{II} = \frac{[R] * [L]}{[RL]} \quad (5)$$

$$K_D^{III} = \frac{[RL] * [C]}{[RLC]} \quad (6)$$

$$K_D^{IV} = \frac{[RC] * [L]}{[RLC]} \quad (7)$$

We define the cooperativity constant α to be the ratio of non-enhanced and enhanced binding:

$$\alpha = \frac{K_D^{I}}{K_D^{III}} = \frac{K_D^{II}}{K_D^{IV}} \quad (8)$$

And replace the equilibrium constants in Eq. 6 & 7:

$$\frac{K_D^I}{\alpha} = \frac{[RL] * [C]}{[RLC]} \tag{9}$$

$$\frac{K_D^{II}}{\alpha} = \frac{[RC] * [L]}{[RLC]} \tag{10}$$

The equilibrium equations can be rewritten to obtain expressions for all complexes [R^{C}], [R^{L}], [R^{LC}] as a function of the dissociation constancy, relevant parameters and free concentration of all species (Eq. 11–13).

$$[RC] = \frac{[R] * [C]}{K_D^I} \tag{11}$$

$$[RL] = \frac{[R] * [L]}{K_D^{II}} \tag{12}$$

$$[RLC] = \frac{[R] * [L] * [C] * \alpha}{K_D^I * K_D^{II}} \tag{13}$$

The equations 11–13 are substituted in the mass-balance equations (Eq. 1-3) to arrive at the following expressions:

$$R_{tot} = [R] + \frac{[R] * [C]}{K_D^I} + \frac{[R] * [L]}{K_D^{II}} + \frac{[R] * [L] * [C] * \alpha}{K_D^I * K_D^{II}} \tag{14}$$

$$L_{tot} = [SL] + \frac{[R] * [L]}{K_D^{II}} + \frac{[R] * [L] * [C] * \alpha}{K_D^I * K_D^{II}} \tag{15}$$

$$C_{tot} = [C] + \frac{[R] * [C]}{K_D^I} + \frac{[R] * [L] * [C] * \alpha}{K_D^I * K_D^{II}} \tag{16}$$

Which can be rewritten to get the expressions for unknown concentrations equilibrium of R, L and C (Eq. 17-19):

$$[R] = \frac{R_{tot}}{1 + \frac{[C]}{K_D^I} + \frac{[S]}{K_D^{II}} + \frac{[S] * [C] * \alpha}{K_D^I * K_D^{II}}} \tag{17}$$

$$[S] = \frac{S_{tot}}{1 + \frac{[R]}{K_D^{II}} + \frac{[R] * [C] * \alpha}{K_D^I * K_D^{II}}} \tag{18}$$

$$[C] = \frac{C_{tot}}{1 + \frac{[R]}{K_D^I} + \frac{[R] * [S] * \alpha}{K_D^I * K_D^{II}}} \tag{19}$$

Custom-written MATLAB scripts are used to solve the coupled non-linear equations 17-19 for the free concentrations R, L and C through recursive interaction (tolerance = 10^-16). Once established, these concentrations are subsequently used to calculate the equilibrium concentrations of all other dependent

species (Eq. 11-13), most importantly the labeled species C, R^C and R^{LC}.From the concentration the modeled anisotropy r_{model} is calculated (Eq. 20). The numerical values for all equilibrium concentrations are filled back into the equilibrium concentration to verify that equilibrium has been reached, as an additional sanity check.

$$r_{model} = \frac{[C]}{C_{tot}} \tag{20}$$

Data analysis and parameter estimation.

We performed non-linear least square analysis on the anisotropy titration data as reported in Figures 2 & 3 in the main manuscript and Supporting Figure S2 by comparing the normalized anisotropy data to the computed anisotropy[1]. Nonlinear least square minimization of the data was performed using the MATLAB function lsqnonlin, a subspace trust region method based on the interior-reflective Newton method. In order to prevent entrapment in a local minimum, 30 different starting values of K_D^{II}, α were defined, and the best fit (defined as the fit with the lowest square of the norm of the residuals) is taken as the final solution for the optimized values. The different initial parameter sets are defined using a latin hypercube sampling method (MATLAB function lhsdesign).

An extended and generalized modeling framework has been made available via https://github.com/TUe-chemical-biology/model-framework

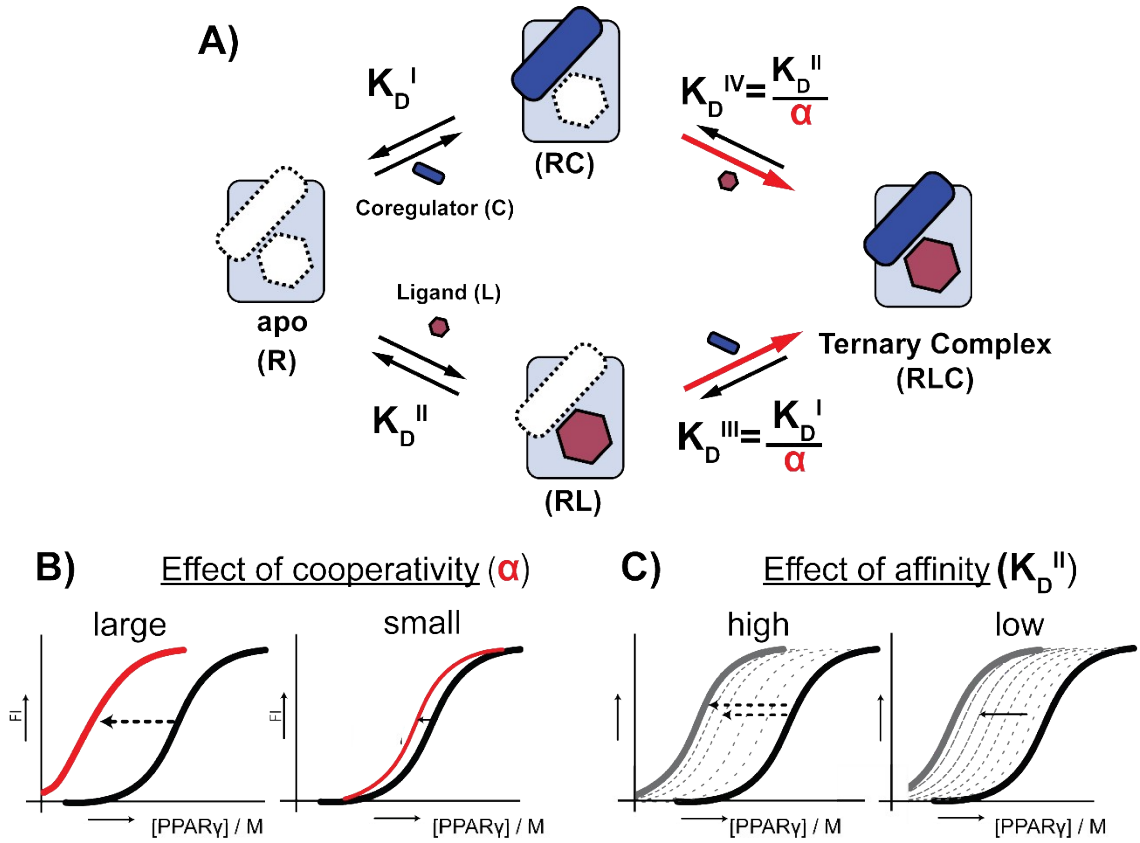

Figure S1. Cooperativity model for nuclear receptor/ligand/coregulator interplay.
A. Cooperativity scheme for ligand coregulatory interplay involving sequential binding events of receptor (R) and ligand (L) and coregulator (C). The binding partner binds to the target protein with K_D^{I} and in the presence of a ligand this affinity is altered to K_D^{I}/α. Similarly, the ligand binds with an intrinsic affinity K_D^{II} and an enhanced affinity K_D^{II}/α when the partner is already bound to the target protein. Mass action laws and mass balance equations allow the creation of a thermodynamic model to obtain numerical values for intrinsic affinity and cooperativity. **B.** Simulated effect of cooperativity on the receptor/co-regulator interaction, upon a saturating dose of ligand (red) versus no ligand (black). A larger cooperativity factor causes a larger the final shift. **C.** Effect of intrinsic affinity (K_D^{II}) shown for a low and high affinity ligand with equal cooperativity. Ultimately, both ligands reach the same effect, but the high affinity ligand reaches this at a lower dose.

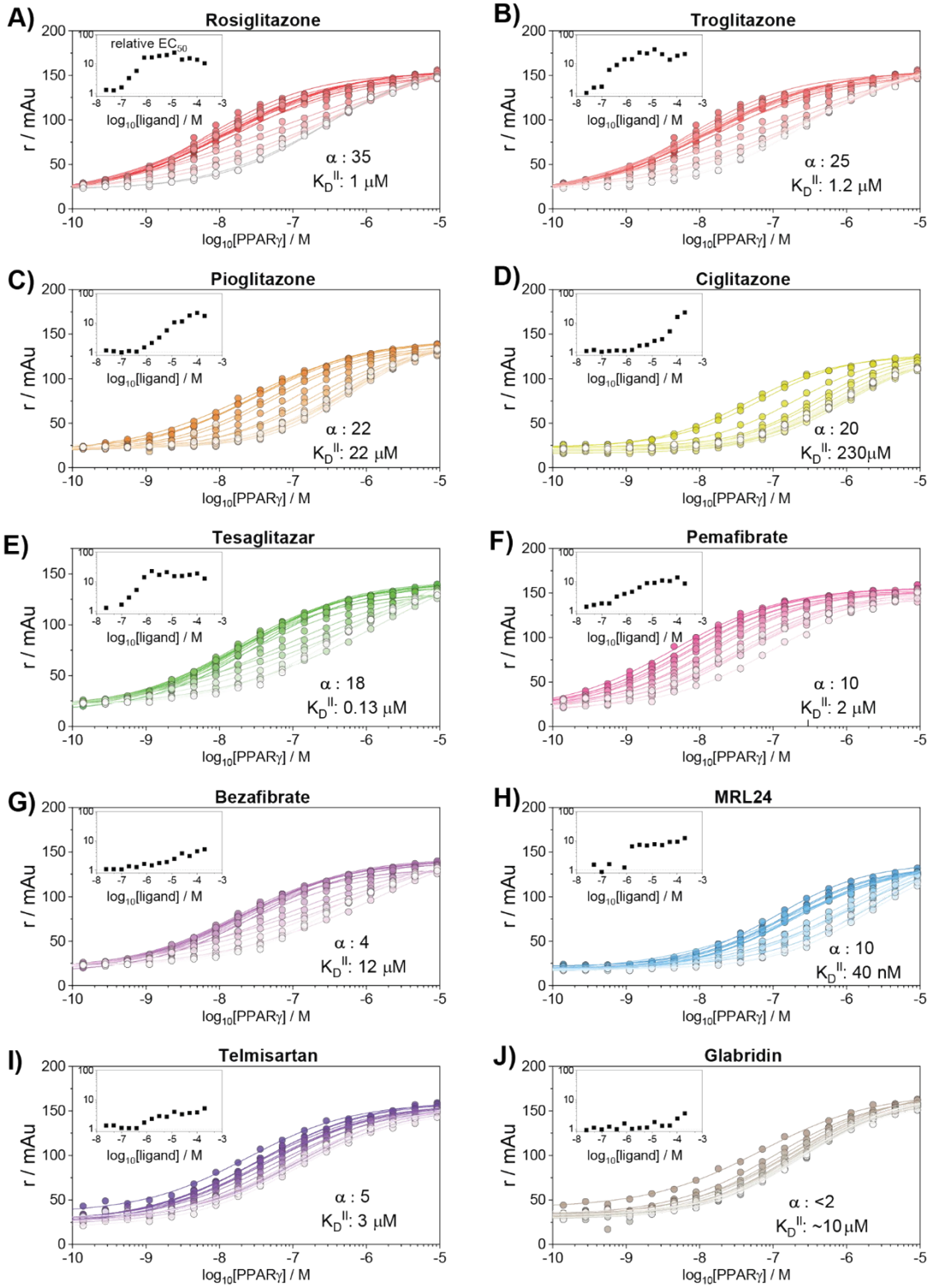

Figure S2. 2D cooperativity analysis of PPARγ agonist on the interaction with the MED1 coregulator. PPARγ is titrated to 10 nM labeled MED1, at several constant concentrations of agonist (0 – 200 μM). Cooperativities and intrinsic affinities parameters. The cooperativity factor α, defined as the ratio between ligand bound affinity and the non-stabilized affinity of the cofactor for the receptor, K_D^{I}/ K_D^{III} is obtained though data-fitting according to the model depicted in Figure 1 of the main text. Insets show to relative EC_{50} as function of the contrition ligand used.

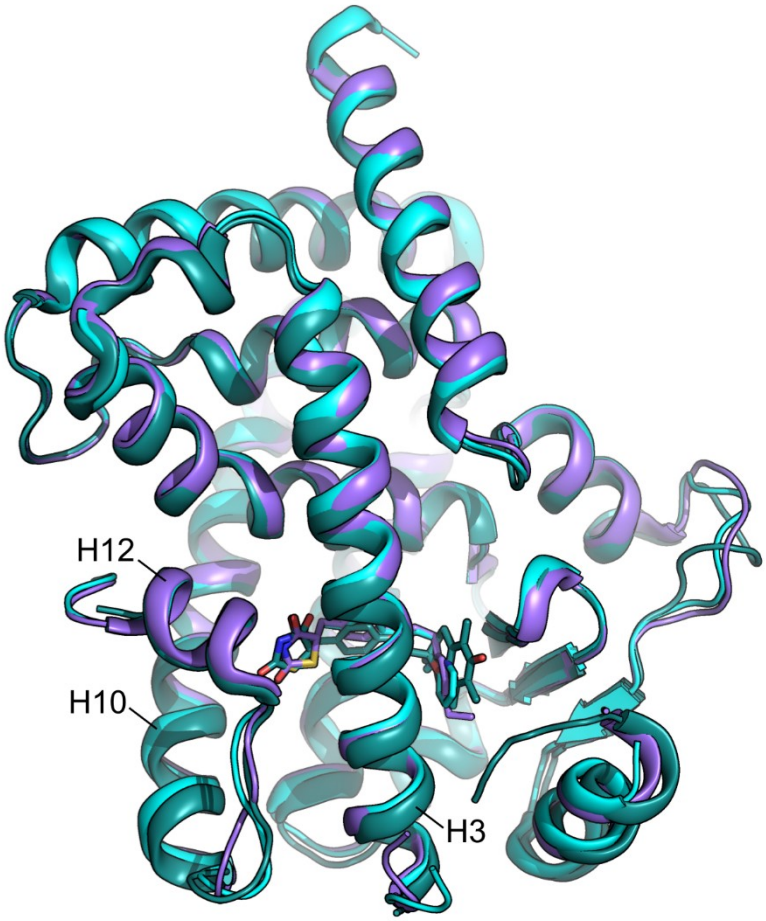

Figure S3. Structural overlay PPARγ in complex with thiazolidinediones. Rosiglitazone in purple (PDB 5YCP); Troglitazone in green (PDB 6DGO) and Pioglitazone in teal (PDB 5Y2O).

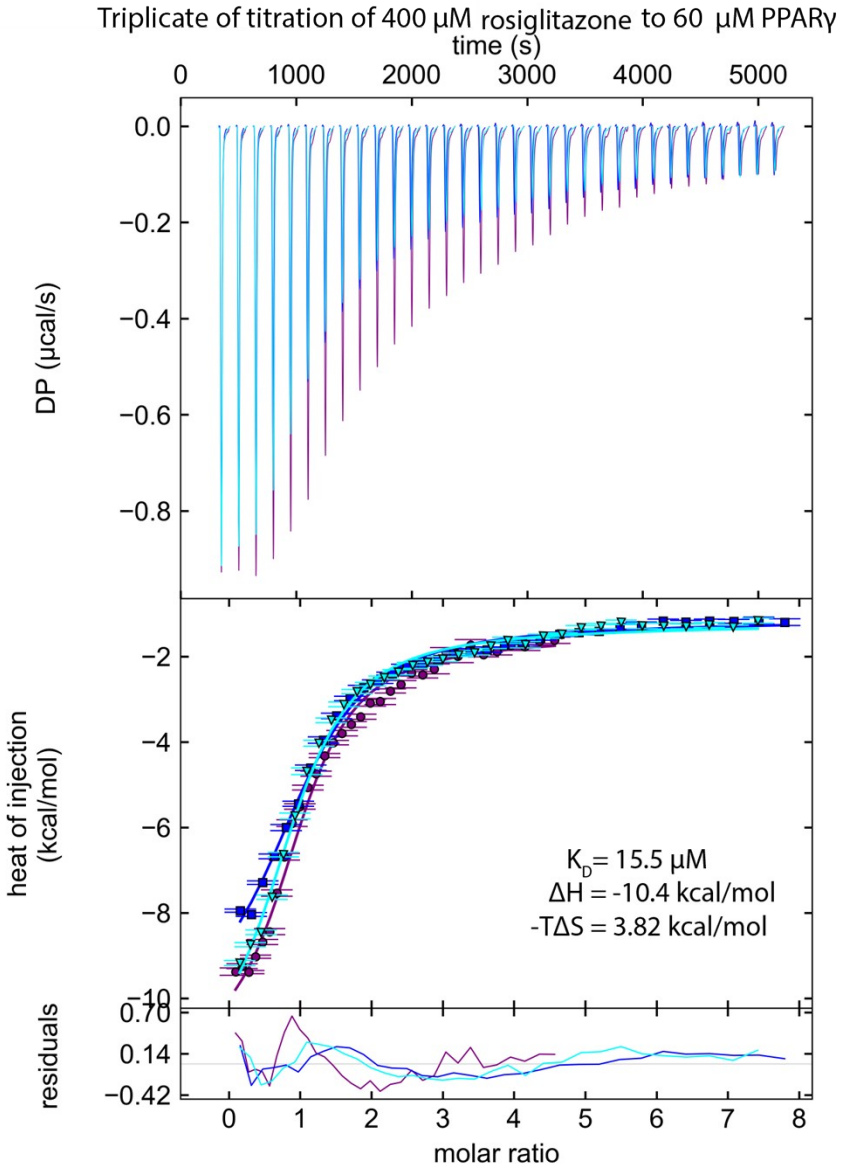

Figure S4. Top: Raw heat measured heat change of injection of rosiglitazone (400 μM in the syringe) to PPARγ-LBD (60 μM). Middle: Normalized measured heats (dots) with best-fit model (line). Parameters were determined from global analysis of triplicate experiment. Incompetent rosiglitazone is considered as a local incompetent fraction. Bottom: Residuals of the fit with a RSMD of 0.433 kcal/mol. The estimated value from global nonlinear analysis for the affinity of rosiglitazone for the apo PPARγ-LBD is 15.5 µM (12.3-18.7 μM) with an enthalpy of 10.4 kcal/mol (+/- 0.4 kcal/mol) reduced $\chi 2$ for this fit is 1.01.

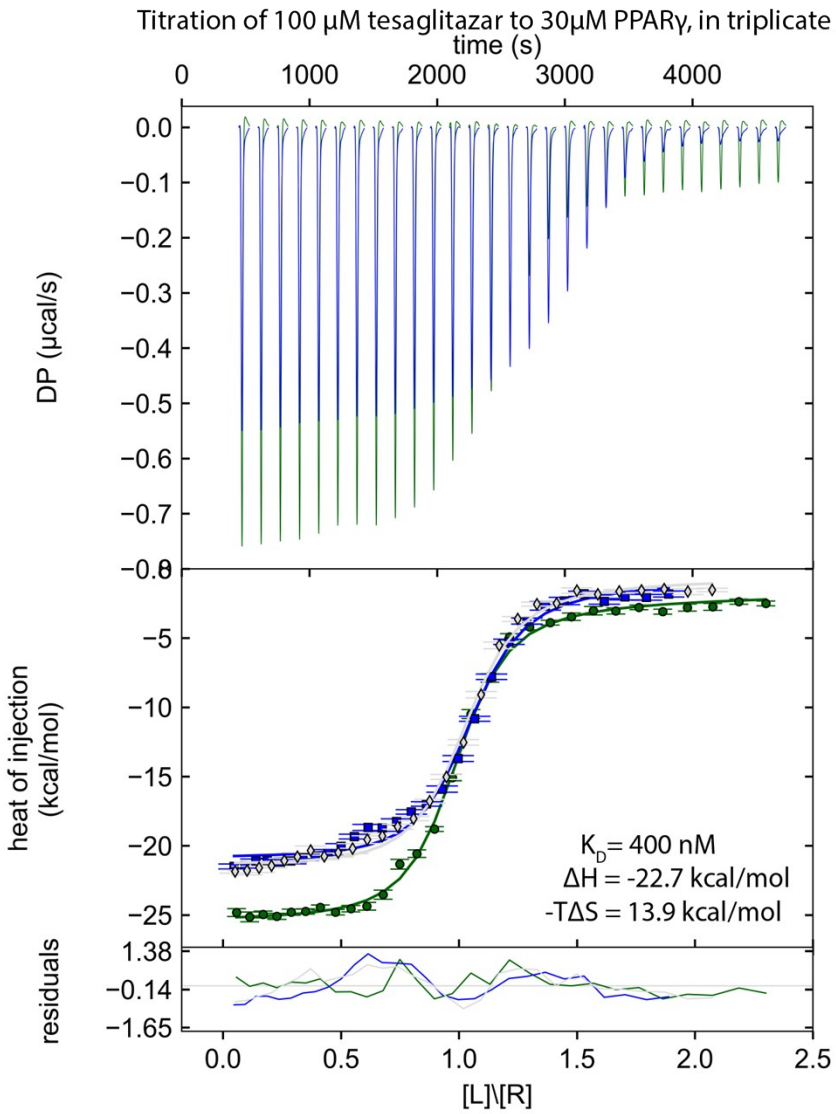

Figure S5. Top: Measured heat change of injection of tesaglitazar (100 µM in the syringe) to PPARy-LBD (30 *µ*M). Middle: Normalized measured heats (dots) with best-fit model (line). Parameters were determined from global analysis of duplicate experiment. Incompetent tesaglitazar is considered as a local incompetent fraction, Bottom: Residuals of the fit with a RSMD of .0.76 kcal/mol. The estimated value of nonlinear analysis for the affinity of tesaglitazar for the apo PPARγ LBD is 400 nM (325-492 nM 95% CI) with an enthalpy of -22.7 kcal/mol (+/- 0.4 kcal/mol) Reduced χ2 for this fit is 0.995.

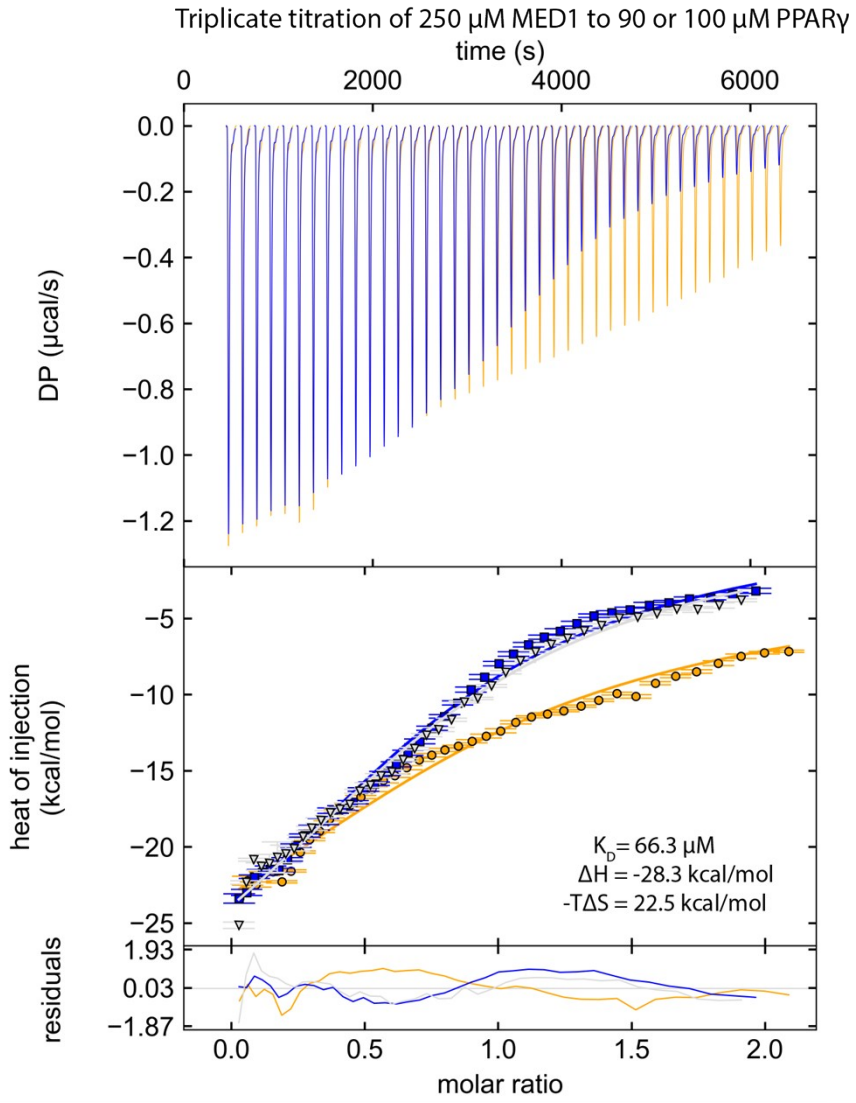

Figure S6. Top: raw heat measured heat change of injection of MED1 peptide (250 µM in the syringe) to PPARγ-LBD (90µM blue and gray, 100 µM yellow). Middle: Normalized measured heats (dots) with best-fit model (line). Parameters were determined from global analysis of triplicate experiment. Incompetent MED1 is considered as a local incompetent fraction. Bottom: Residuals of the fit with a RSMD of 0.90 kcal/mol. Affinity derived from non-linear analysis: Kd: 66.3 µM (49.2-89.4 µM 95% CI) enthalpy -28.3 kcal/mol (-25.7 / -31.7 kcal/mol 95% CI) reduced global $\chi 2$ of 2.95.

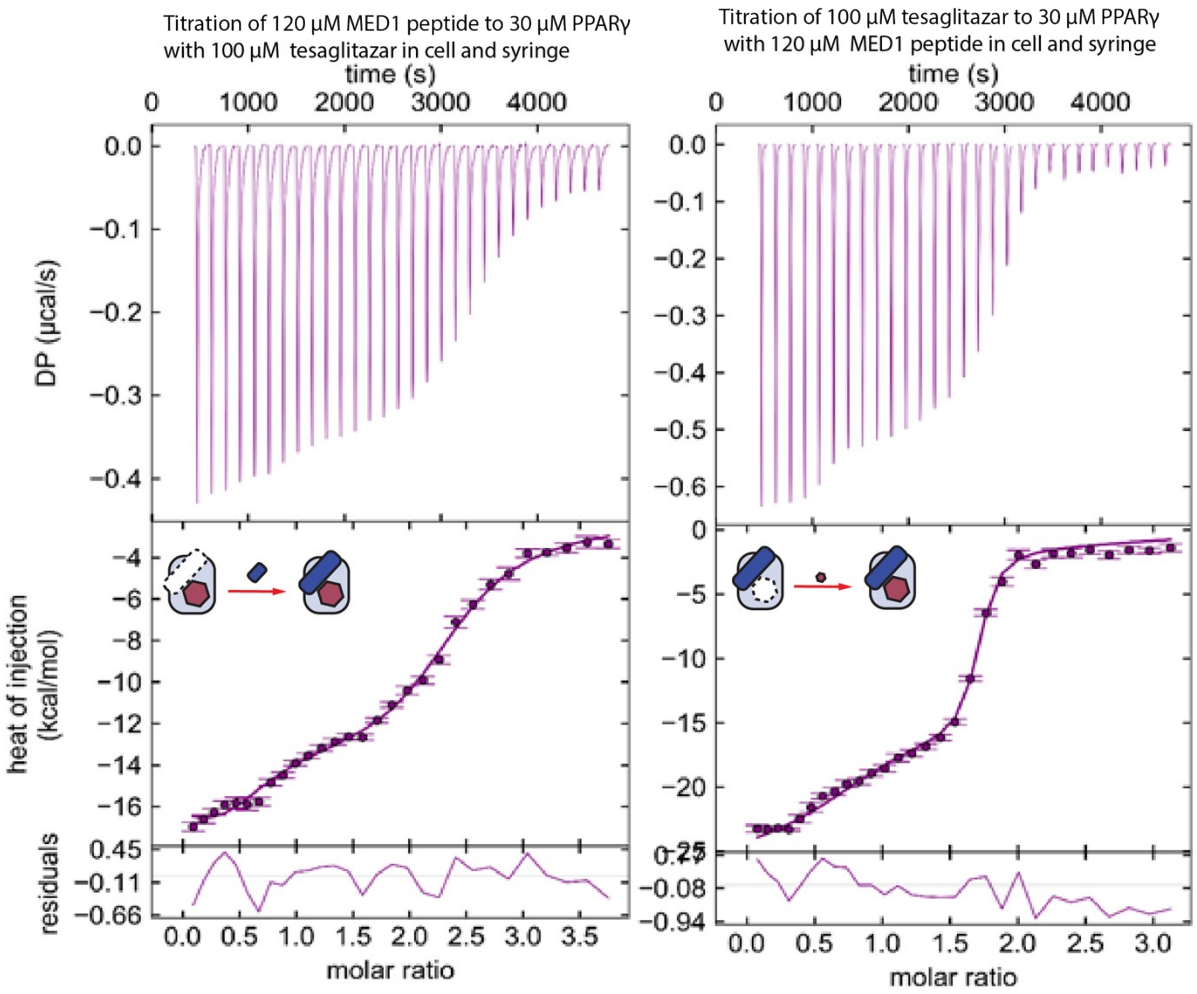

Figure S7. Top left: Measured heat change of injection of MED1 peptide (120 µM in the syringe) to PPARy-LBD (30 µM) with 100 µM tesaglitazar in both cell and syringe. Top right: Measured heat change of injection of tesaglitazar (100 µM in the syringe) to PPARy-LBD (30 µM) with 120 µM MED1 in both cell and syringe middle: Normalized measured heats (dots) with courtesy-fit (line).

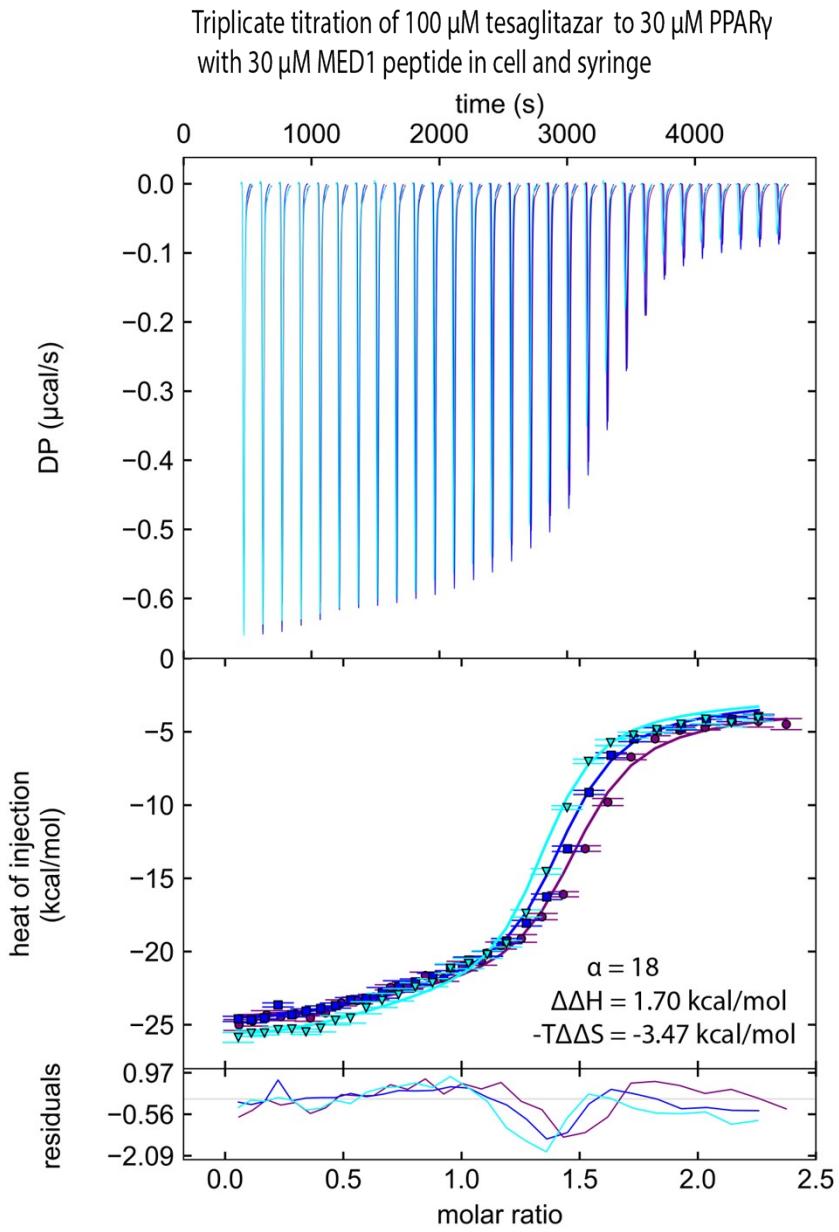

Figure S8. Top: Measured heat change of injection of tesaglitazar (100 µM in syringe) to PPARy-LBD (30 µM) with 30 µM MED1 in both cell and syringe. Middle: Normalized measured heats (dots) with best-fit model (line). Parameters were determined from global analysis of duplicate experiment. Parameter for both binary interactions are obtained from previous experiments and treated as prior knowledge. Incompetent tesaglitazar is considered as a local incompetent fraction, incompetent MED1 is considered as a global incompetent fraction. Bottom: Residuals of the fit with a RSMD of 0.73 kcal/mol. The cooperativity value for tesaglitazar is 18 (15-22 95%CI) The reduced χ^2 of the fit is 0.951

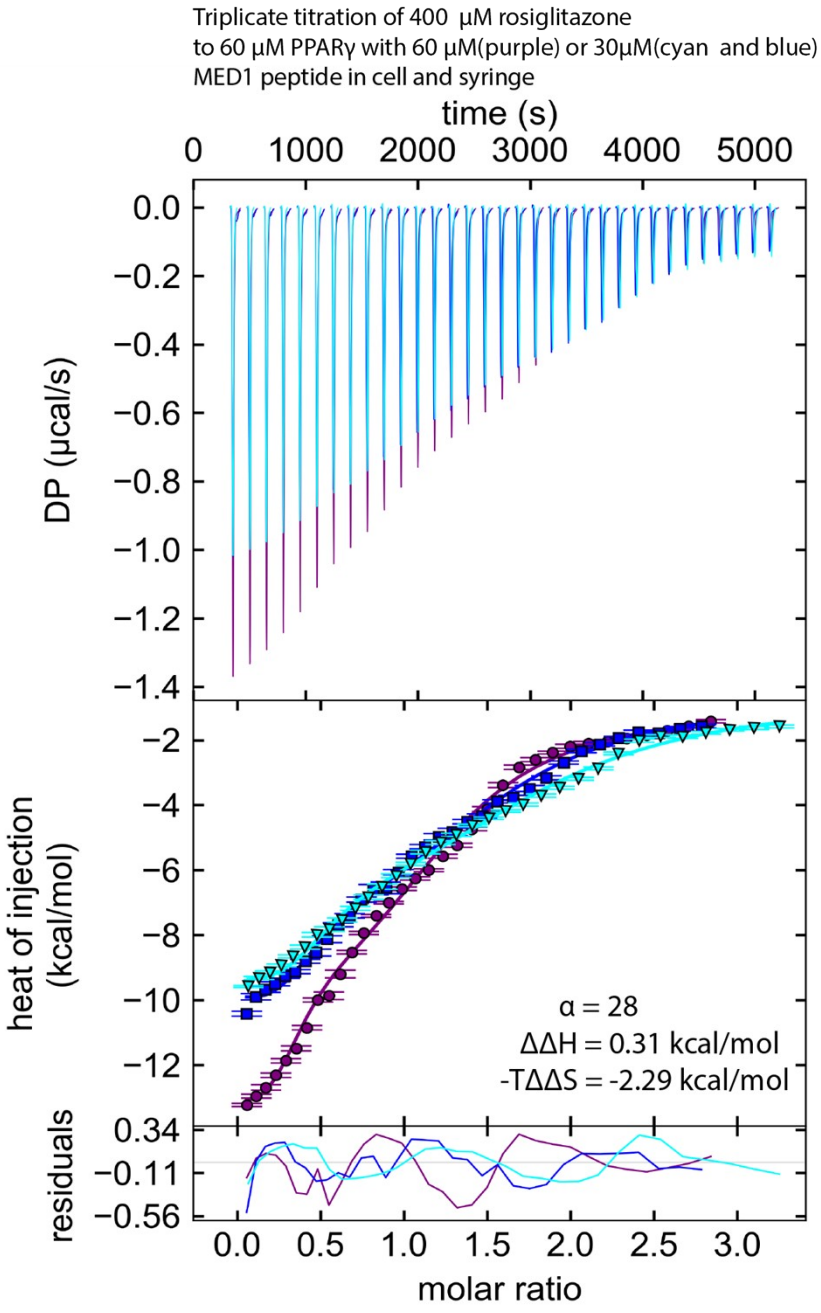

Figure S9. Top: Measured heat change of injection of rosiglitazone (400 µM in the syringe) to PPARy-LBD (60 µM) with 60 µM MED1 in both cell and syringe. Middle: Normalized measured heats (dots) with best-fit model (line). Parameters were determined from global analysis of duplicate experiment. Parameter for both binary interactions are obtained from previous experiments and treated as prior knowledge. Incompetent tesaglitazar is considered as a local incompetent fraction, incompetent MED1 is considered as a global incompetent fraction. Bottom: Residuals of the fit with a RSMD of 0.73 Rosiglitazone has a cooperativity value of 28 (22-34 95% CI). The reduced χ^2 of the fit is 1.97

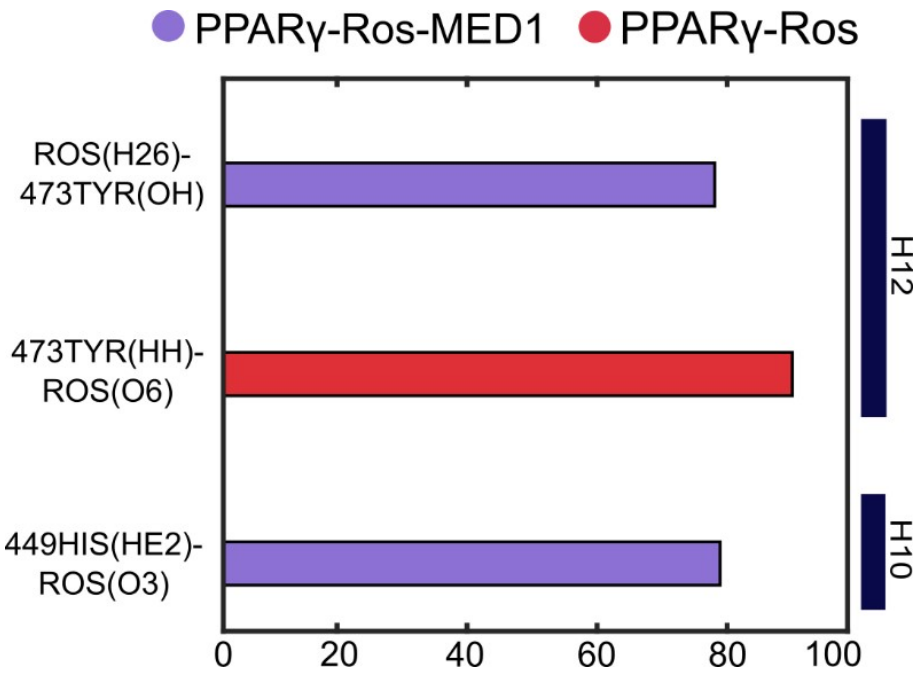

Figure S10. Hydrogen bonds between Rosiglitazone and PPARγ. On the left, the comparison of the occupancy (%) of the hydrogen bonds in the presence (●) and in the absence (●) of the coregulator.

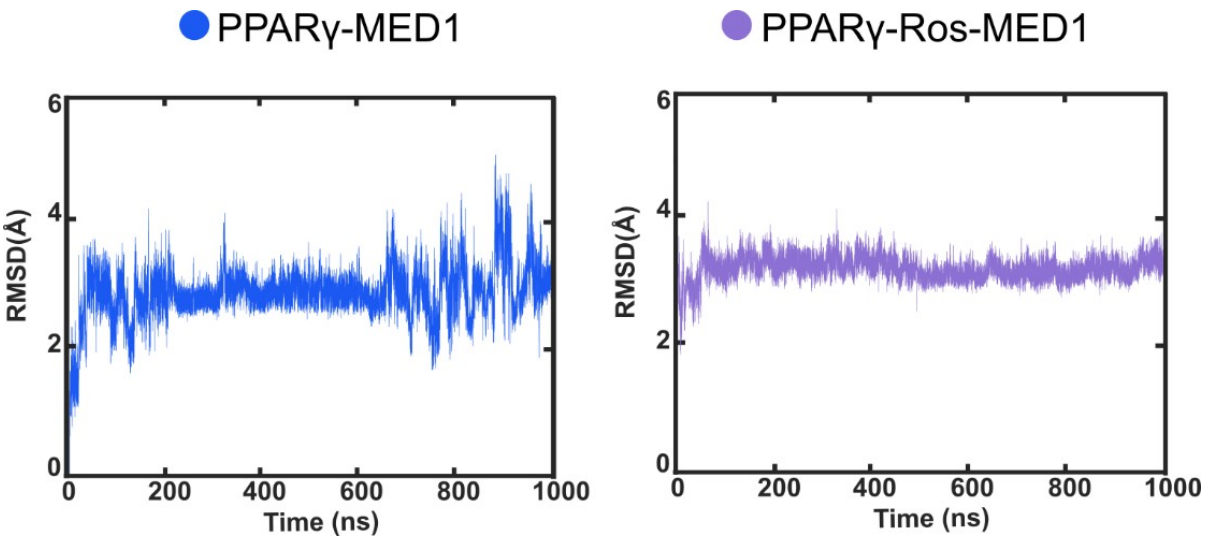

Figure S11. RMSD plot of MED1 in the absence (●) and in the presence (●) of the ligand.

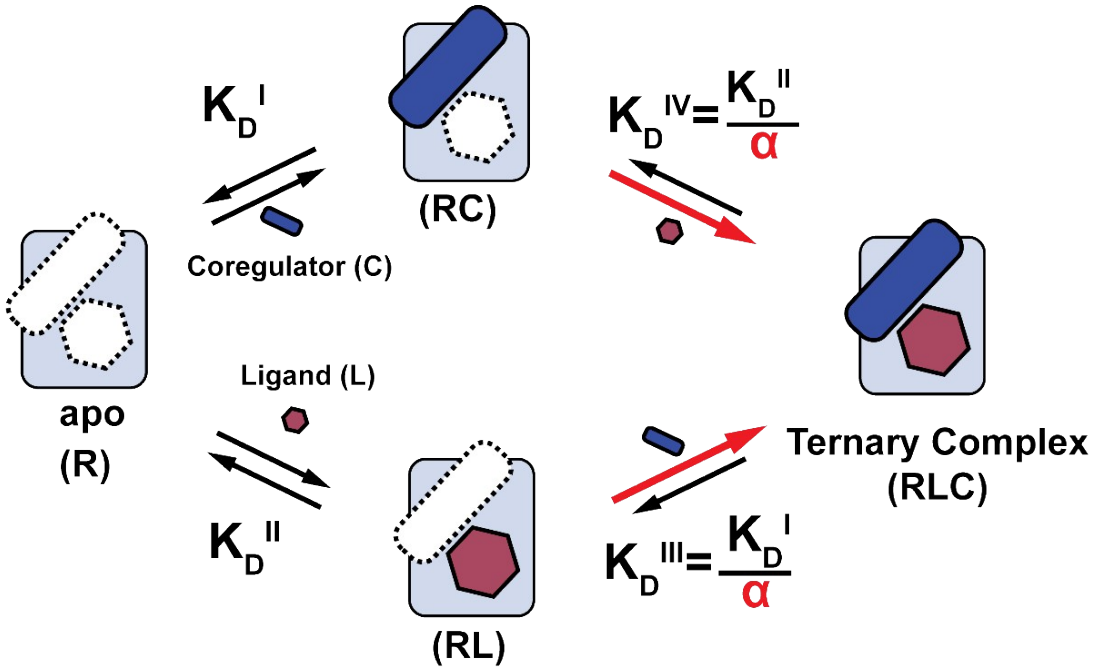

Figure S12. Cooperativity scheme for ligand coregulator interplay involving sequential binding events of receptor (R) and ligand (L) and coregulator (C). The coregulator binds to the target protein with K_D^{I} and in the presence of a ligand this affinity is altered to K_D^{I}/α. Similarly, the ligand binds with an intrinsic affinity K_D^{II} and an enhanced affinity K_D^{II}/α when the coregulator binding partner is already bound to the target protein. Mass action laws and mass balance equations allow the creation of a thermodynamic model to obtain numerical values for intrinsic affinity and cooperativity.

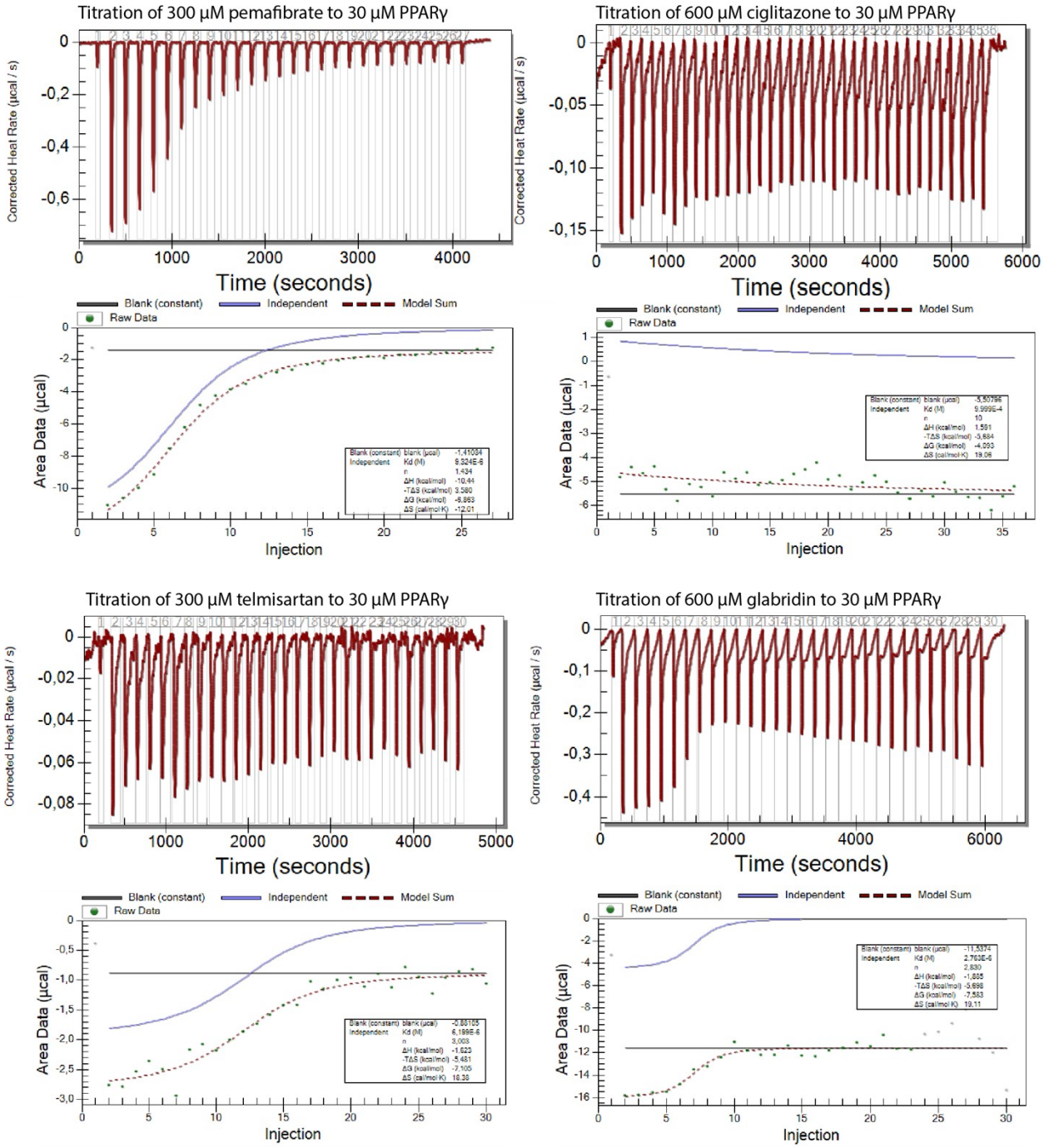

Figure S13A. Measured raw thermograms, binding isotherms and derived thermodynamic values for pioglitazone, bezafibrate, MRL24 and troglitazone, as presented in table S.1 and main text. Used concentrations are above each graph. A constant blank model is used to correct for heat of injection (grey line), independent model is used to model ligand binding(blue), model sum is depicted as dashed red line.

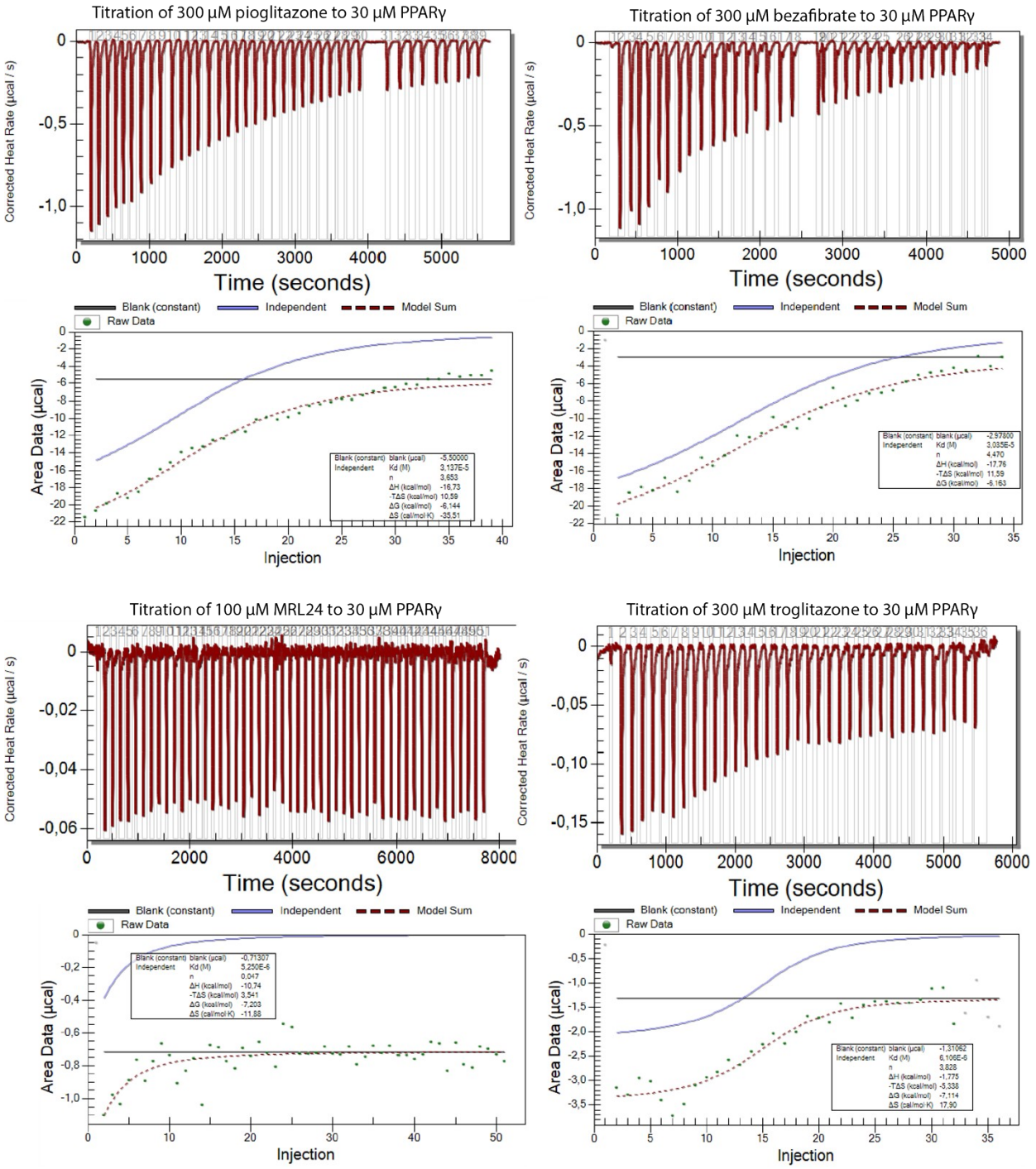

Figure S13B. Measured raw thermograms, binding isotherms and derived thermodynamic values for pemafibrate, ciglitazone, telmisartan and glabridin, as presented in table S.1 and main text. Used concentrations are above each graph. A constant blank model is used to correct for heat of injection (grey line), independent model is used to model ligand binding(blue), model sum is depicted as dashed red line.

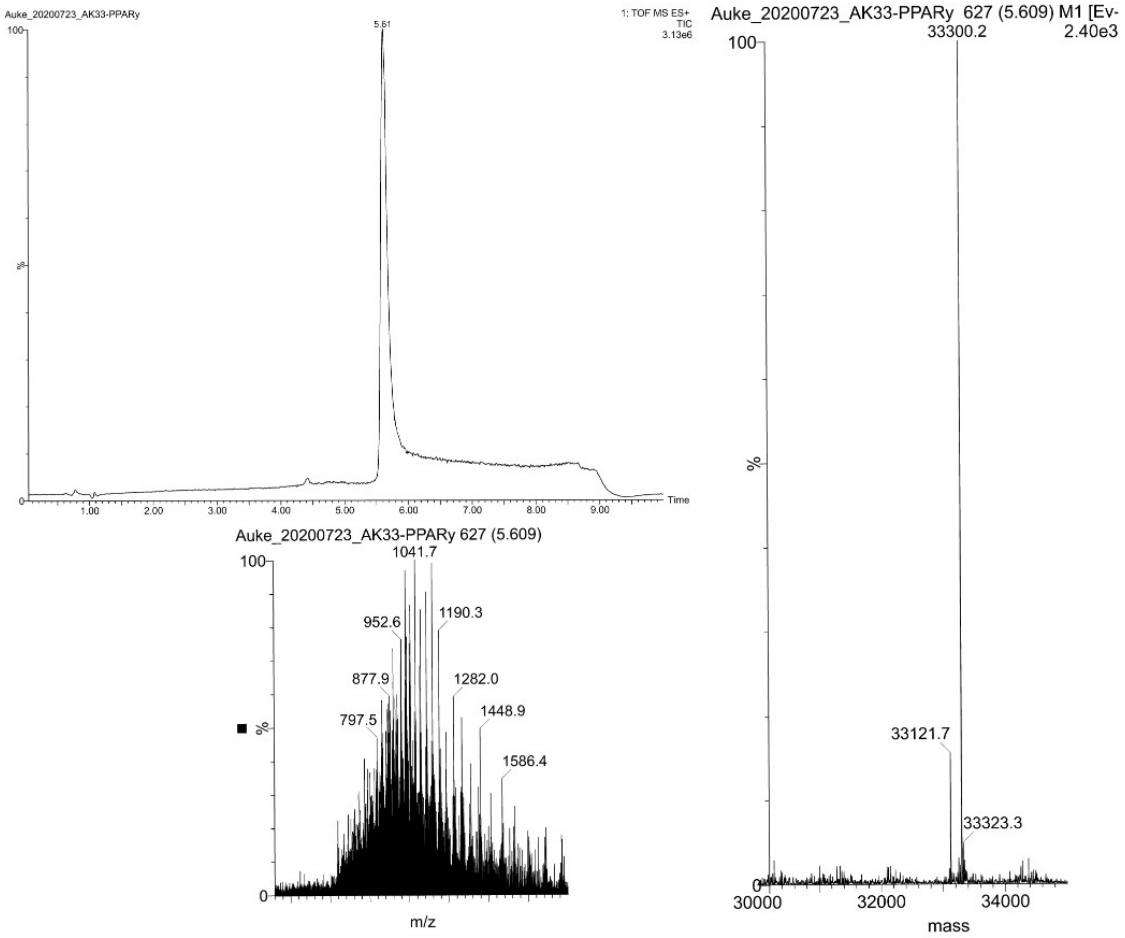

Figure S14. Top left; Chromatogram of PPARy-LBD sample. Protein elutes at 5.81 min and single elution peak confirms protein purity. Bottom left; m/z spectrum of elution peak. Right; deconvuluted m/z spectrum. The mass of 33121.7 is the mass of the construct, without the first methionine. Peak of 33300.2 is a posttranslational histag modification, small adjacent peak is the sodium adduct of 33300.

Sequence of PPARγ-LBD as expressed in E.coli BL21 DE3 using a pET15-b vector, with his-tag en thrombin cleavage site. Residue numbering is according to isoform 1.

MGSSHHHHHHSSGLVPRGSHME$_{207}$*SADLRALAKHLYDSYIKSFPLTKAKARAILTGKTTDKSPFVIYDMNS LMMGEDKIKFKHITPLQEQSKEVAIRIFQGCQFRSVEAVQEITEYAKSIPGFVNLDLNDQVTLLKYGVHEIIY TMLASLMNKDGVLISEGQGFMTREFLKSLRKPFGDFMEPKFEFAVKFNALELDDSDLAIFIAVIILSGDRPG LLNVKPIEDIQDNLLQALELQLKLNHPESSQLFAKLLQKMTDLRQIVTEHVQLLQVIKKTETDMSLHPLLQEI YKDLY*$_{477}$

Table S1. Overview of isothermal titration calorimetry characteristics of agonist to PPARγ

Ligand	**K_D / μM**	**N**	**ΔG / kcal·mol^{-1}**	**ΔH / kcal·mol^{-1}**	**-TΔS / kcal·mol^{-1}**
Rosiglitazone	15.5	1.57 0.95 1.02	-6.58	-10.42	3.8
Troglitazone	6.11	3.82	-7.11	-1.78	-5.4
Pioglitazone	31.3	3.65	-6.14	n.d.	n.d.
Ciglitazone	n.d.	n.d.	n.d.	n.d.	n.d.
Tesaglitazar	0.400	1.31 1.45 1.35	-8.82	-22.70	13.9
Pemafibrate	9.03	1.43	-6.86	-10.44	3.6
Bezafibrate	30.3	4.47	-6.16	n.d.	n.d.
MRL24	n.d.	n.d.	n.d.	n.d.	n.d.
Telmisartan	7.96	3.00	-7.11	-1.62	-5.5
Glabridin	14.6	2.83	-7.59	-1.86	-5.7

n.d. = not determined.

Table S2. Hydrogen bonds occupancy between MED1 and PPARγ in the ternary complex. The bonds in common between the two states are highlighted.

Hydrogen Bond	%Occupancy
642HIE(HE2) - 468LEU(O)	**92.0**
640LYS(HZ1) - 399GLY(O)	37.4
640LYS(HZ1) - 316THR(OG1)	32.8
640LYS(HZ1) - 313ASP(OD2)	47.4
640LYS(HZ1) - 313ASP(OD1)	34.7
640LYS(HZ1) - 312ASN(OD1)	16.7
320TYR(HH) - 639THR(O)	56.3
319LYS(HZ1) - 641ASN(O)	59.6
319LYS(HZ1) - 638THR(O)	50.6
316THR(HG1) - 640LYS(O)	19.6
301LYS(HZ1) - 651ASP(O)	11.9
301LYS(HZ1) - 648LEU(O)	**46.8**
638ASN(D21) - 268GLU(O)	24.4

Table S3. Hydrogen bonds occupancy between MED1 and PPARγ in the binary complex. The bonds in common between the two states are highlighted.

• Hydrogen Bond	• %Occupancy
• **642HIE(HE2) - 468LEU(O)**	• **17.4**
• 642HIE(H) - 471GLU(OE2)	• 22.0
• 642HIE(H) - 471GLU(OE1)	• 13.3
• 641ASN(D21) - 471GLU(OE2)	• 14.3
• 641ASN(D21) - 316THR(OG1)	• 27.5
• 641ASN(D21) - 312ASN(OD1)	• 40.1
• 641ASN(H) - 312ASN(OD1)	• 18.4
• 639THR(H) - 399GLY(O)	• 19.4
• 638ASN(D21) - 402ASN(O)	• 21.1
• 638ASN(D21) - 313ASP(OD1)	• 27.7
• 402ASN(H) - 638ASN(OD1)	• 22.3
• 401LEU(H) - 275ASN(OD1)	• 19.5
• 312ASN(D21) - 638THR(O)	• 28.4
• 301LYS(HZ1) - 650LYS(O)	• 10.2
• **301LYS(HZ1) - 648LEU(O)**	• **38.5**

SI References.

(1) de Vink, P. J.; Andrei, S. A.; Higuchi, Y.; Ottmann, C.; Milroy, L.-G.; Brunsveld, L. Cooperativity Basis for Small-Molecule Stabilization of Protein–Protein Interactions. *Chemical Science* **2019**, *10*, 2869–2874. https://doi.org/10.1039/C8SC05242E.

(2) Wolter, M.; de Vink, P.; Neves, J. F.; Srdanović, S.; Higuchi, Y.; Kato, N.; Wilson, A.; Landrieu, I.; Brunsveld, L.; Ottmann, C. Selectivity via Cooperativity: Preferential Stabilization of the P65/14-3-3 Interaction with Semisynthetic Natural Products. *J. Am. Chem. Soc.* **2020**, *142* (27), 11772–11783. https://doi.org/10.1021/jacs.0c02151.

(3) Scheuermann, T. H.; Brautigam, C. A. High-Precision, Automated Integration of Multiple Isothermal Titration Calorimetric Thermograms: New Features of NITPIC. *Methods* **2015**, *76*, 87–98. https://doi.org/10.1016/j.ymeth.2014.11.024.

(4) Brautigam, C. A. Calculations and Publication-Quality Illustrations for Analytical Ultracentrifugation Data. *Methods Enzymol* **2015**, *562*, 109–133. https://doi.org/10.1016/bs.mie.2015.05.001.

(5) Jang, J. Y.; Bae, H.; Lee, Y. J.; Choi, Y. I.; Kim, H.-J.; Park, S. B.; Suh, S. W.; Kim, S. W.; Han, B. W. Structural Basis for the Enhanced Anti-Diabetic Efficacy of Lobeglitazone on PPARγ. *Sci Rep* **2018**, *8* (1), 31. https://doi.org/10.1038/s41598-017-18274-1.

(6) Jacobson, M. P.; Friesner, R. A.; Xiang, Z.; Honig, B. On the Role of the Crystal Environment in Determining Protein Side-Chain Conformations. *J Mol Biol* **2002**, *320* (3), 597–608. https://doi.org/10.1016/s0022-2836(02)00470-9.

(7) Jacobson, M. P.; Pincus, D. L.; Rapp, C. S.; Day, T. J. F.; Honig, B.; Shaw, D. E.; Friesner, R. A. A Hierarchical Approach to All-Atom Protein Loop Prediction. *Proteins* **2004**, *55* (2), 351–367. https://doi.org/10.1002/prot.10613.

(8) Shang, J.; Mosure, S. A.; Zheng, J.; Brust, R.; Bass, J.; Nichols, A.; Solt, L. A.; Griffin, P. R.; Kojetin, D. J. A Molecular Switch Regulating Transcriptional Repression and Activation of PPARγ. *Nat Commun* **2020**, *11* (1), 956. https://doi.org/10.1038/s41467-020-14750-x.

(9) Hess, B.; Kutzner, C.; van der Spoel, D.; Lindahl, E. GROMACS 4: Algorithms for Highly Efficient, Load-Balanced, and Scalable Molecular Simulation. *J Chem Theory Comput* **2008**, *4* (3), 435–447. https://doi.org/10.1021/ct700301q.

(10) Mark, P.; Nilsson, L. Structure and Dynamics of the TIP3P, SPC, and SPC/E Water Models at 298 K. *The Journal of Physical Chemistry A* **2001**, *105* (43), 9954–9960.

(11) Wang, J.; Wolf, R. M.; Caldwell, J. W.; Kollman, P. A.; Case, D. A. Development and Testing of a General Amber Force Field. *Journal of Computational Chemistry* **2004**, *25* (9), 1157–1174. https://doi.org/10.1002/jcc.20035.

(12) Bayly, C. I.; Cieplak, P.; Cornell, W.; Kollman, P. A. A Well-Behaved Electrostatic Potential Based Method Using Charge Restraints for Deriving Atomic Charges: The RESP Model. *J. Phys. Chem.* **1993**, *97* (40), 10269–10280. https://doi.org/10.1021/j100142a004.

(13) Decherchi, S.; Bottegoni, G.; Spitaleri, A.; Rocchia, W.; Cavalli, A. BiKi Life Sciences: A New Suite for Molecular Dynamics and Related Methods in Drug Discovery. *J. Chem. Inf. Model.* **2018**, *58* (2), 219–224. https://doi.org/10.1021/acs.jcim.7b00680.